THz Time-Domain Spectroscopy For Dummies

by Dima Fishman

For many decades researchers have studied the dynamics of carriers. A very interesting region for these studies is the far-infrared or submillimeter region, where the frequency of the electromagnetic radiation is comparable to the carrier damping rate. A potential disadvantage of regular optical pump-probe experiments is that the probe energy, typically 1.5 eV or higher, is much larger than the relevant energy scales in many systems. Combining THz time-domain spectroscopy with optical excitation one can measure the evolution of optically induced changes in the real and imaginary part of the dielectric function with a probe energy much closer to the relevant energy scale in the material.

A typical example of mid-infrared reflectivity spectra in condensed phase calculated by Nagai *et. al.* [1] is displayed in Fig. 1. The reflectivity has a very distinctive response in the case of different concentrations and spatial distributions of the photo-excited carriers: it is flat for a low density of carriers (1); it has a Drude like shape for a high carrier density uniformly distributed over the sample (2) and it displays a resonance for a high density of carriers, gathered in ”droplets” in-homogeneously distributed throughout the sample. This example demonstrates the possibility of using optical-pump THz-probe spectroscopy in order to induce and see the signature of a metal to insulator transitions for example: in the case of a metal one would see a Drude like sample response, while in the case of an insulator a flat response will be observed.

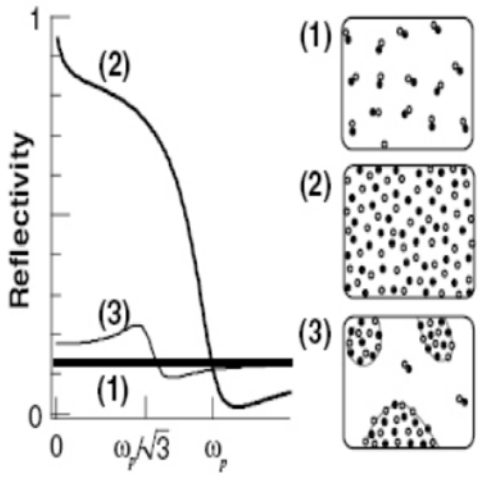

Fig. 1. Typical response from different spatial distributions of photo-excited carriers in an mid infrared pump-probe experiment. Reflectivity around plasma frequency $\hbar\omega_p$ at different distributions of electron-hole: (1) dilute excitonic gas, (2) homogenous plasma, and (3) electron-hole droplet [1].

Generation and detection of one/few cycle terahertz pulses.

Since the emergence of terahertz spectroscopy, in the middle of 80's, there was a continuous process of searching for new materials with efficient emission of terahertz radiation. In parallel, an improvement process regarding the useful THz radiation bandwidth was taking place. As a result, today, a multitude of methods and materials are used for the generation of THz frequencies. Between them, the use of photoconductive antenna's based on low-temperature-grown GaAs and Si-GaAs is the oldest method for generating and detecting THz pulses, [2-4]. THz radiation can result also from transient conductivity which is based on high-intensity ultrashort laser pulses exciting the surface of an unbiased semiconductor [5]. Synchrotrons and free electron lasers can generate short pulses of far-infrared radiation, typically on the order of 5 -10 ps. It has been shown that laser-generated plasmas can produce radiation up to 4 THz, [6,7]. More recently, there have been notable developments in using a single structure for transmitter and receiver, named transceiver and based on electro-optic crystals, [8]. In this case, the electro-optic terahertz transceiver alternately transmits pulsed electromagnetic radiation (optical rectification) and receives the return signal (electro-optic effect) using the same crystal.

Still, probably the most popular choice for high energy THz pulse generation, when working with amplified laser systems, is to employ optical rectification in a nonlinear medium. The nonlinear medium is in most of the cases ZnTe but GaAs and GaP have been used as well. It has been shown that organic molecular crystals like DAST [9] and MBANP [10] are also capable of generating THz pulses by optical rectification. They are more efficient than ZnTe crystals of the same thickness, but are more fragile and cannot withstand high energy fluxes.

The optical rectification process can be understood as the difference frequency analogue of second harmonic generation. In other words, when light interacts with a nonlinear medium and wave mixing between two frequencies, ω_1 and ω_2 occurs, the result is sum-frequency generation, $\omega_1+\omega_2$, and difference frequency generation, $\omega_1-\omega_2$. In the particular case when $\omega_1=\omega_2$, one generates both second harmonic and DC pulses. Because the near-IR pulse has a duration of 80 fs, a "DC" pulse corresponding to the envelope of the optical generating pulse rather than a constant dc level.

Alternatively, this generation mechanism can be understood by considering the fact that the optical pulses have significant bandwidths. Thus, the high-frequency components can mix with the low-frequency components within a given pulse to produce a pulse at the difference frequency (Fig. 2). Since the optical pulses have a bandwidth of a few THz, the difference frequencies fall in the THz range. Difference frequency mixing produces a low frequency polarization which follows the envelope of the incident laser pulse.

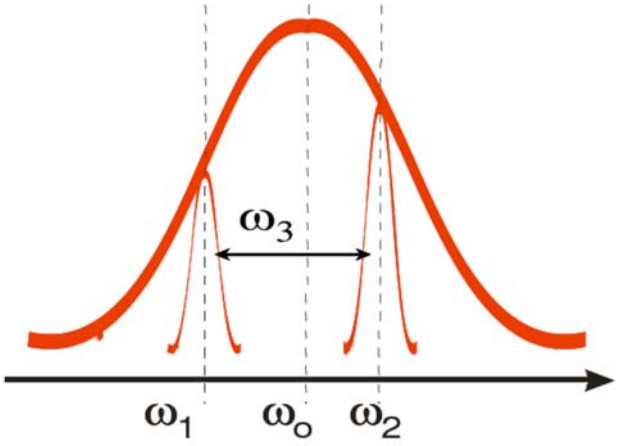

Fig. 2. The low frequency component of a pulse ω_1, and the high frequency component ω_2, are mixing, producing a pulse at the difference frequency $\omega_3=\omega_1-\omega_2$.

One advantage of optical rectification is that it is a non-resonant process and the THz pulse width is limited only by the optical laser pulse width as well as optical phonon absorption of the crystal, but not the response time of the media. Some of the shortest THz pulses to date, with bandwidths up to 100 THz and beyond have been generated in this or a similar fashion [11-13]. Kubler *et. al.* have used a 20 µm thick GaSe crystal to generate THz pulses with a bandwidth beyond 120 THz, [11]. In a THz spectrometer, the generated radiation bandwidth can be tuned between 2.5 THz and 100 THz, by choice of the appropriate nonlinear medium and optical generating pulse length.

Once the THz pulses have been generated, the need for a reliable detection scheme becomes a must. The conventional approach is the photoconductive antenna [2-4, 11], based on low-temperature-grown GaAs and Si-GaAs. When a high-power low-repetition rate experiment or a destructive experiment is performed, a single-shot detection is desirable (it is possible to collect an entire THz waveform without having to scan a delay line) [14-17]. Nahata and Heinz have demonstrated that it is possible to detect THz pulses via optical second harmonic generation [18]. Polarization modulation, as opposed to amplitude modulation, when using optoelectronic detection has also been demonstrated [19].

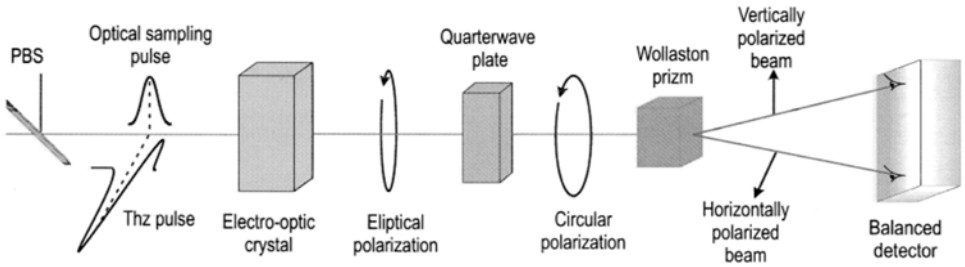

Fig. 3. Schematics of free space electro-optic sampling detection. PBS – pellicle beam splitter.

When using an amplified laser system, the pulses are detected best via free space electrooptic sampling rather than photoconductive dipole antennas (PDA's) [12-20]. Due to non-resonant nature of the process the potential for damaging the detector crystal with the focused readout beam is much lower. The FSEOS is based on the electric field of a THz pulse inducing a small birefringence in an electro-optic crystal through a non-linearity of the first order (Pockels effect). Passing through such crystal, the initially linearly polarized optical probe beam gains a small elliptical polarization. In the first approximation, this ellipticity is proportional to the electric field applied to the crystal, i.e. to the THz pulse in every certain moment of time. Because the THz field is much longer than the optical probe pulse (several ps versus ~80 fs), the THz electric field can be approximated as a DC bias field. Therefore, varying the delay between the THz and optical probe pulse, the whole time profile of the first can be traced. As an FSEOS active medium, a variety of dielectric materials like LiTaO3 and ZnTe [21, 22] or polymers polarized by externally applied field [22, 23] are employed.

In practice, a quarter-wavelength plate is placed behind the electro-optic crystal to make the initially linear polarization of the probe beam (at $E_{THz} = 0$) circular (Fig. 3). A Wollaston prism separates its orthogonal components and sends them to a balanced differential detector which is connected to a preamplifier and a lock-in amplifier. With no THz present, the components have equal intensity and the differential signal is zero.

Terahertz time-domain spectrometer

Typical THz spectrometer is driven by a femtosecond amplifier and very schematically depicted in Fig. 4. The emitter crystal is [110]-oriented and 1 mm thick. Detection is made using a [110]-oriented ZnTe crystal of 0.2 mm mounted on a [100]-oriented ZnTe crystal of 0.5 mm. When a short microwave pulse is applied on the detection crystal, the group-velocity mismatching of ZnTe must be considered. The measured group-velocity mismatching of ZnTe is 0.4 ps/mm. In order to reduce walk-off for better temporal resolution, the thinner [110] crystal provides shorter convolution window (about 0.1 ps), and the thicker [100] crystal delays the reflected THz pulse, with no contribution to the electrooptic phase retardation. The disadvantage of using a thinner crystal is the reduction of electrooptic signal, due to the shorter interaction length [21].

The 80 fs laser pulse with the central wavelength around 800 nm excites a transient nonlinear polarization spike in the emitter ZnTe crystal, which produces an electromagnetic pulse with the frequency spectrum in the THz range. The THz pulse is guided to the detector ZnTe crystal by the off-axis parabolic mirrors. Once the THz pulse is transmitted to the surface of the detector ZnTe crystal, its electric field induces a birefringence in this crystal. This birefringence is detected by the phase retardation of the very weak 800 nm laser probe pulse which has a pre-aligned polarization. This probe laser pulse is temporally delayed with respect to the pump laser used for THz generation using the variable delay line. It is therefore possible to measure the phase retardation (which is proportional to the electric field of the THz pulse) with a time resolution of about 80 fs. After the propagation through the $\lambda/4$ plate, the phase-retarded optical probe pulse will become elliptically polarized, which will result in different light intensities incident on the two photodiodes of the differential detector. The difference in voltages detected by these photodiodes will be proportional to the induced phase retardation and, therefore, to the electric field strength in the THz pulse. Varying the delay between the THz pulse and the optical probe one can therefore temporally sample the electric field in the THz pulse.

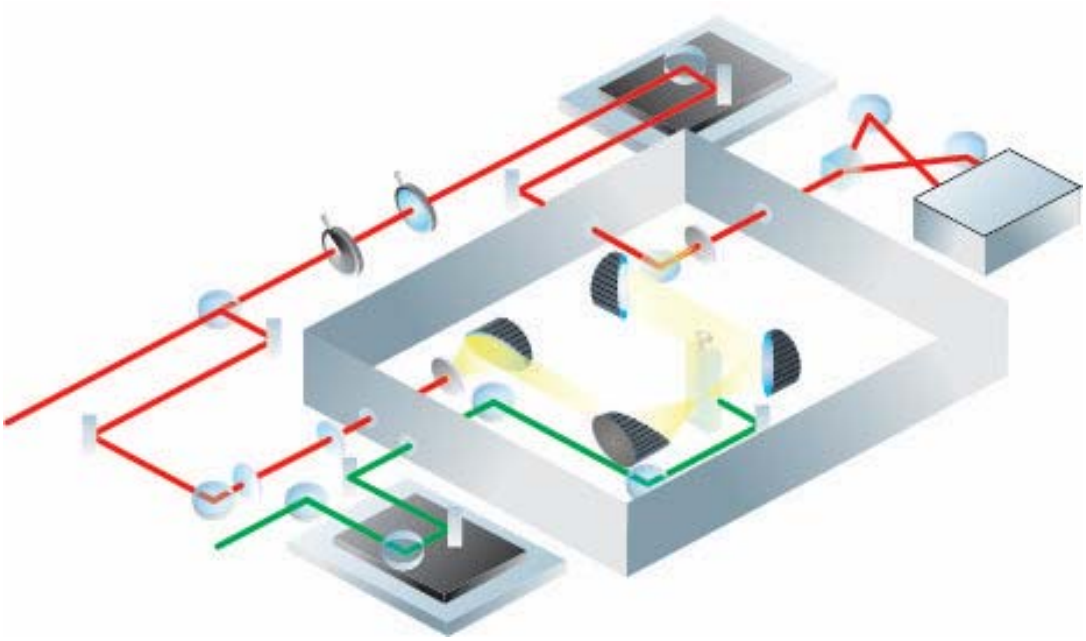

Fig. 4. Schematic representation of the terahertz time-domain transmission spectrometer.

The measured electric field in the THz pulse in the case of the FSEOS in cubic electrooptic crystals can be estimated as, [1]:

$$E_{THz} = \frac{2\Delta V}{V_{\max}} \frac{c}{\omega n_0^3 r_{41} d}, \qquad (1)$$

where ΔV is the difference in the voltages detected by the two photodiodes of the differential detector. *Vmax* is the voltage produced by each of the photodiodes when they are illuminated with the probe beam, when no THz field is applied. Then $\Delta V = Vmax - Vmax = 0$. n_0 and r_{41} are the refractive index and the electrooptic coefficient of the nonlinear crystal at the frequency of the probe beam ω, d is the thickness of the crystal. For the ZnTe crystal probed at 800 nm n_0=3.22, [23].

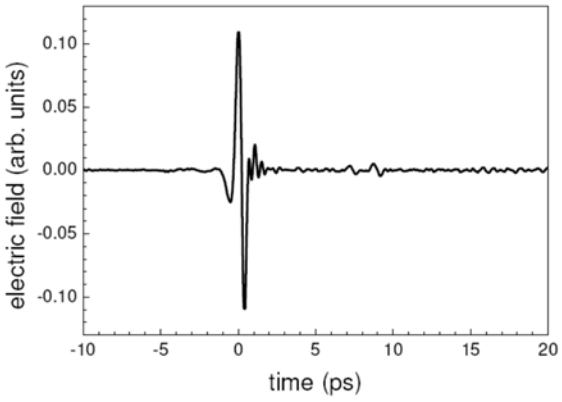

Fig. 5. Time trace of a typical terahertz pulse obtained with our THz spectrometer.

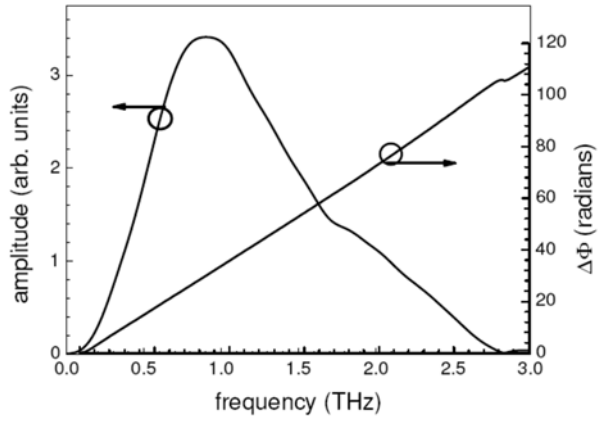

Fig. 6. Amplitude and phase of the terahertz time trace Fourier transform.

THz generation by optical rectification of ultrashort laser pulses was first demonstrated by the group of Y. R. Shen in 1971 [24]. The FSEOS detection scheme was first introduced by the groups of X. C. Zhang [21] and P. Uhd Jepsen and H. Helm [25] in 1996. Both these techniques are widely used ever since and allow for coherent detection of the electric field temporal evolution in ultrashort transients. Recently the generation and detection of THz pulses with the peak electric field strength of the order of 1 MV/cm was demonstrated using optical rectification and FSEOS detection schemes, [12]. A typical time trace of a THz pulse generated and detected in our THz spectrometer is shown in Fig. 5, while it's amplitude and phase frequency dependent spectra are shown in Fig. 6. This pulse was generated by the 800 nm central wavelength , 150 fs long laser pulse with the fluence of approximately 0.5 mJ/cm2.

The THz pulse has a relatively complicated shape with a main single-cycle oscillation, followed by decaying an-harmonic oscillations. The maximum signal-to-noise (S/N) ratio of this pulse is about 10^3. This THz pulse has a useful bandwidth in the range 0.1-2.5 THz, which is considerably smaller than the bandwidth of the 150 fs excitation laser pulse. The temporal shape and bandwidth of a THz pulse produced by optical rectification in an optically transparent nonlinear crystal is determined by the temporal shape and bandwidth of the excitation pulse as well as by the phase mismatch between the optical and THz pulses copropagating through the crystal and the THz absorption by phonons in the crystal.

Propagation of an electromagnetic wave packet through the medium. Terahertz spectral analysis.

Now, let's concentrate over the propagation of a linearly polarized electromagnetic pulse through a plan-parallel slab of dispersive medium, i.e. a medium with frequency-dependent refractive index and absorption coefficient. Fig. 7 is a schematic representation of the propagation of a THz pulse through the sample with frequency dependent refractive index *n(ω)* and power absorption coefficient *α(ω)*. The free-space signal $\hat{E}_r$ does only suffer changes caused by the optical components encountered during propagation. We call this changes the system response. The sample signal $\hat{E}_s$, however, does experience, besides the system response, reflection losses at the sample's interfaces as well as absorption and chirp inside the sample. The extraction of the dielectric properties of the sample, such as refractive index and power absorption coefficient requires a change from the time-domain to the frequency-domain, which is done using Fourier transformation. In the following equations all parameters are frequency-dependent. The detected THz signals propagated through the free-space $\hat{E}_r$ and through both free-space and sample $\hat{E}_s$ have a complex form:

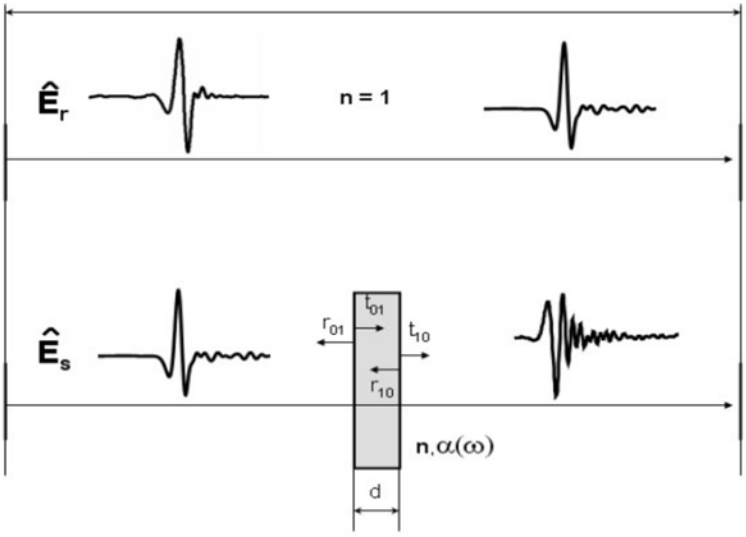

Fig. 7. $\hat{E}_r$ and $\hat{E}_s$ are the THz signals transmitted through the free space (reference pulse) and through the free space and sample. R is the length of the optical path between emitter and detector and d is the sample thickness. r_{01}, t_{01} and r_{10}, t_{10} are the amplitude reflection and transmission coefficients at the front and the back of the sample, respectively. n(ω) and α(ω) are the frequency dependent refractive index and power absorption coefficient of the sample.

$$\begin{aligned} \hat{E}_r &= E_0 e^{ikr} = E_0 e^{i\phi_{free}} \\ \hat{E}_s &= E_0 t_{01} t_{10} e^{ik(r-d)} e^{i\tilde{n}kd} = E_s e^{i\phi_{sample}}, \end{aligned} \qquad (2)$$

In this equations E_0 is the electric field strength of the reference pulse, $k=\omega/c$ is the free space wavevector, r is the length of the optical path, d is the sample thickness, $\tilde{n}=n+i\kappa$ is the sample

complex refractive index, and t_{01} and t_{10} are the amplitude transmission coefficients at the front and back surfaces of the sample, respectively. The electric fields $\hat{E}_s$ and $\hat{E}_r$ in complex form are defined by their amplitude and phases E_s, ϕ_{sample} and E_0, ϕ_{free}.

The amplitude reflection and transmission coefficients at the front and back surfaces of the sample in the case of normal incidence are:

$$\begin{aligned} r_{01} &= \frac{1-\breve{n}}{1+\breve{n}} \quad t_{01} = 1 + r_{01} \\ r_{10} &= \frac{\breve{n}-1}{1+\breve{n}} \quad t_{10} = 1 + r_{10}, \end{aligned} \tag{3}$$

Knowing that the power absorption coefficient $\alpha = 2k\kappa$ and taking into account Eq. 3 we can write the ratio of the electric fields $\hat{E}_s$ and $\hat{E}_r$ as:

$$\frac{\hat{E}_s}{\hat{E}_r} = \frac{4\breve{n}}{(1+\breve{n})^2} e^{-\frac{\alpha}{2}d} e^{i(\bar{n}-1)kd} = \frac{E_s}{E_0} e^{i(\phi_{sample}-\phi_{free})}, \tag{4}$$

Performing a complex fit of the experimentally obtained transmission with the theoretical one displayed in Eq. 4, the real and imaginary refractive index, n and κ are obtained.

The real refractive index and the absorption coefficient, α, can also be obtained considering the following approximation: neglecting the losses suffered due to absorption at the air - sample interfaces (i.e. taking κ=0 in the first term of Eq. 4). This approximation is valid in the case of relatively low-absorbing samples of any thickness, or optically thick but relatively high-absorbing samples. In this case, the refractive index in Eq. 4 will became real (the absorptive component κ is neglected) and the transmission becomes:

$$\frac{\hat{E}_s}{\hat{E}_r} = \frac{4n}{(1+n)^2} e^{-\frac{\alpha}{2}d} e^{i(n-1)kd} = \frac{E_s}{E_0} e^{i(\phi_{sample}-\phi_{free})}, \tag{5}$$

$$n = \frac{\phi_{sample} - \phi_{free}}{\frac{2\pi f}{c} d} + 1, \tag{6}$$

Therefore from the measured phase difference of the sample and reference pulses, and taking into account that $\omega = 2\pi f$, f being the frequency, one can obtain the frequency dependent real part of the refractive index:

Having calculated the refractive index one can separate the reflection and absorption losses in the sample. The power absorption coefficient of the sample will be then:

$$\alpha = -\frac{2}{d} \ln\left[\frac{E_s}{E_0} \frac{(1+n)^2}{4n} \right], \tag{7}$$

In Fig. 8 example of THz pulse transmitted through 1 mm thick direct band-gap semiconductor crystal is shown, using a 1 mm thick [110]-oriented ZnTe crystals for emission and a double ZnTe crystal: a 0.2 mm [110] oriented crystal glued on a 0.5 mm [100] for detection.

The sample THz pulse's zero level was manually displaced from that of the reference in the figure for clarity. The time *t=0* has been chosen to be the time where the main peak of the THz pulse is placed. In the beginning and the end, both pulses have been zeroed. One can notice that the main feature of the sample signal appears approximately 4 ps later than the main feature of the reference pulse, so one could immediately estimate $n_{sample}(THz)$ using the simple relation $\Delta t=(n-1)d/c$ (where *d* is the sample thickness and *c* is the speed of light in vacuum) to find *n*=2,7. This sample pulse delay results from the propagation through the sample, which refractive index is greater than 1. It has smaller amplitude and its shape is distorted in comparison to the reference pulse. This results from the frequency dependent absorption coefficient and refractive index of the semiconductor crystal. In the sample signal, a main THz peak appears at 4 ps followed by another feature at 10 ps distance. This feature originates from the etalon reflection in the plan parallel sample, i.e. it is a part of the main THz signal after it made a round trip in the sample. Knowing the sample refractive index we can calculate that in order to travel two sample lengths, the THz reflected pulse will need approximately 9,82 ps. The etalon reflection might be suppressed or removed by using a wedged sample. This echo signal has a distorted time shape and is much weaker than the main pulse. Nevertheless, if Fourier transform of the THz transient and the echo is performed, the echo will influence the transform, leading to an incorrect spectrum. In order to avoid this inconvenient, one can pad the echo part of the time-domain THz signal with zeroes, since the oscillations from the main pulse are already strongly damped at this point. The time-domain THz signal with a zero-padded echo part is shown by the solid line in Fig. 8.

Fig. 9 presents the amplitude spectra of the reference and sample THz pulses as well as the phase difference induced by the propagation through the sample in the frequency domain. The amplitude spectra have their maxima at around 1 THz. The reference and sample amplitude spectra have a cut-off frequency of approximately 2.5 THz. As discussed before, the limitation of the reference spectrum is related to the process of generation and detection in ZnTe crystals. The noise floor is approximately 0,0025, which makes the maximum amplitude dynamic range (DR) of about 400 for the reference and the sample spectra.

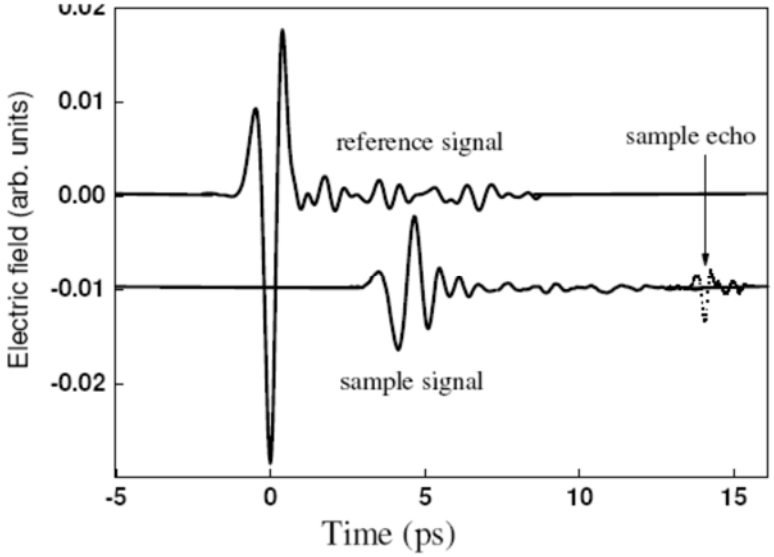

Fig. 8. THz-TDS on a 1 mm semiconductor crystal at room temperature. Measured THz time-domain signals: raw reference signal (upper solid line), raw sample signal (lower dashed line) and sample with removed emitter echo (lower solid line). The time-domain signals were vertically separated for clarity. time t=0 is chosen to be the time where the main peak of the THz pulse is located.

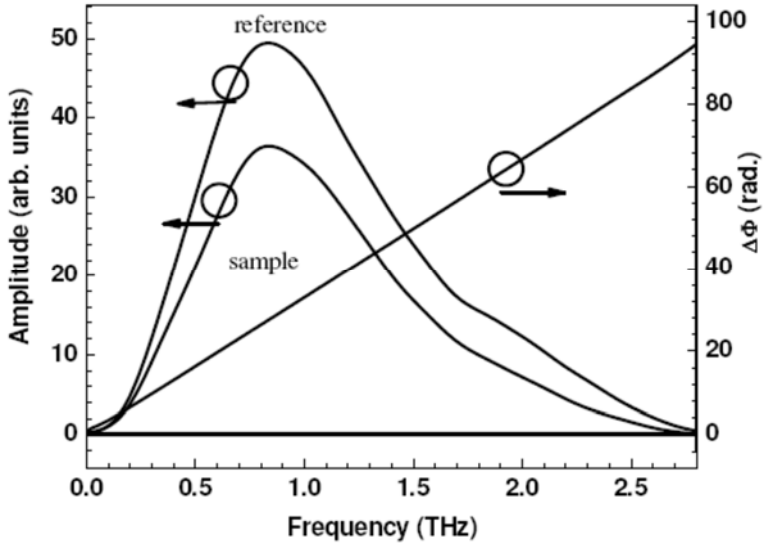

Fig. 9. Frequency domain amplitude reference and sample (with the echo parts removed) and the phase difference between them.

In Fig. 10 and Fig. 11 the refractive index and absorption spectra are shown. These refractive index and absorbtion spectra are calculated from the amplitude and phase spectra using Eq. 7 and Eq. 8. As was shown by Jepsen and Fischer [30], one can define the frequency-dependent dynamic range of the measured absorption spectrum based on the signal-to-noise consideration.

The maximal frequency-dependent absorption coefficient that can be reliably measured with THz-TDS follows from Eq. 8:

$$\alpha_{\max} = -\frac{2}{d}\ln\left[DR\frac{4n}{(1+n)^2}\right], \qquad (8)$$

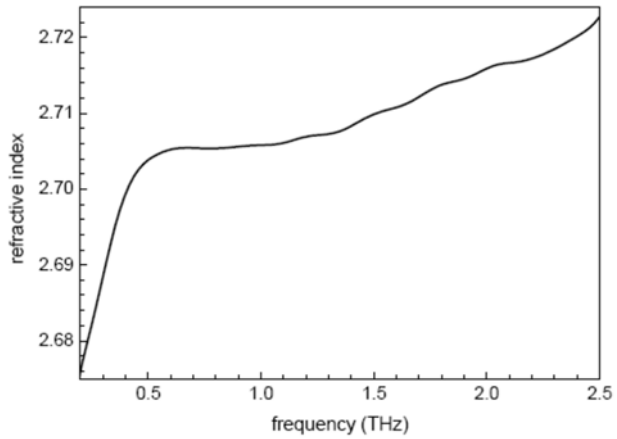

Fig. 10. Frequency dependent refractive index calculated from the amplitude and phase spectra.

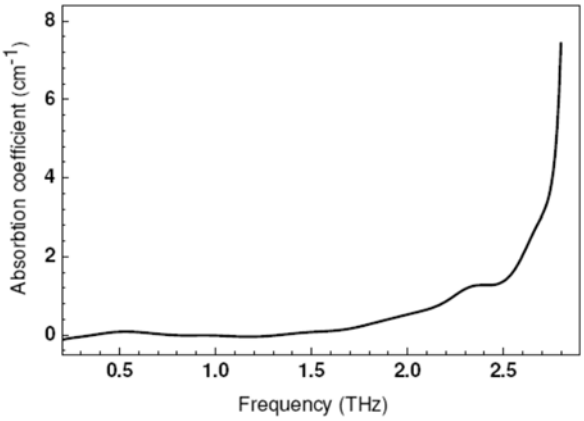

Fig. 11. Power absorption coefficient calculated from the amplitude and phase spectra.

where *d* is the sample thickness, *DR* is the frequency-dependent dynamic range, and *n* is the frequency-dependent refractive index.

The frequency resolution of the THz-TDS is given by the time step and the number of data points in the time-domain measurement $\Delta f = 1/Ndt$, where *N* is the number of data points in the THz time-domain signal and *dt* is the time step. Fast Fourier transform method (FFT) is used to perform the Fourier transforms numerically and proved to be excellent when the number of data points *N* is a power of 2. In the measurements presented above the raw data consists of 625 data points with a time step of 40 fs, thus making the whole time scan of 25 ps. In order to reach the nearest power of 2 value which is 1024, the time-domain signals were padded with zeroes after the last measured data point. The reference signal was padded with zeroes already after the

532th data point in order to avoid the Fabry-Perot effects in the frequency domain caused by the echo of the sample (Fig. 8). This operation did not affected the integrity of the measured and calculated data, because in this range there was already no signal above the noise related to the main THz oscillation. Thus, the frequency resolution of these experiment is Δf =0,04 THz. It should be mentioned that the zero padding and removal of the echoes in the time-domain data should be performed very carefully because if the meaningful part of the original signal is cut, the frequency domain data will contain false features and lack the true ones.

Time-resolved optical-pump terahertz-probe spectroscopy and 2D-Raman.

In optical-pump THz-probe and 2D-Raman experiments, an intense optical pump pulse, derived from the same laser beam that triggers the THz transmitter and detector, perturb the sample. Through delay, the optically induced changes in the transmitted electric field can be measured with femtosecond resolution. The complex sample signal as a function of frequency and pump-probe delay time τ is given by:

$$S(\omega,\tau)=\frac{FFT(E_{eq}(t)+\Delta E(t,\tau))}{FFT(E_{ref}(t))}=\frac{E_{sig}(\omega,\tau)}{E_{ref}(\omega)}, \qquad (9)$$

where $E_{eq}(t)$ is the equilibrium scan of the sample in the time-domain without optical excitation, $\Delta E(t,\tau) = E_{ex}(t,\tau)-E_{eq}(t)$ is the induced change in the electric field with $E_{eq}(t,\tau)$ being the scan of the sample with optical excitation.

Experimentally, $\Delta E(t,\tau=\tau_l)$ is obtained by scanning the THz probe delay line and mechanically chopping the optical pump delay line which is positioned at a specific pump-probe delay time τ_l. This procedure measures the difference between $E_{ex}(t,\tau_l)$ and $E_{eq}(t)$ at the rate of the chopper frequency immediately yielding $\Delta E(t,\tau=\tau_l)$ at each THz probe delay time t_r. Alternatively, by chopping and scanning the THz probe delay line one would collect the data for $E_{ex}(t,\tau_l)$ (i.e. pump on) and $E_{eq}(t)$ (i.e. pump off) in separate scans. The direct measurement of $\Delta E(t,\tau)$ allows for increased signal sensitivity as it is more robust to system drift, particularly when the induced change is small. Then the real and imaginary part of the dielectric function can be obtained through a procedure which was given in the previous section. After obtaining $\Delta E(t,\tau=\tau_l)$, $E_{eq}(t)$ and $E_{ref}(t)$ are measured by chopping and scanning the THz probe delay line. $\Delta E(t,\tau=\tau_l)$ must be measured at each pump-probe delay time because the optical excitation can induce changes in both the phase and amplitude of the THz field. However, for samples in which the optical excitation produces changes primarily in the amplitude of the THz electric field, an alternative method can be used. $\Delta E(t_{peak},\tau)$ as a function of τ is obtained in a single scan by chopping and scanning the optical pump delay line while the THz delay line is positioned at the peak of the THz electric field. This method, if applicable, can provide considerable time savings in measuring the induced dynamics. It must be kept in mind that this proceeding is an approximation which can be employed only when the induced change is small, or when the phase of the THz pulse does not change with optical excitation. This method is in most of the cases not applicable, because t_{peak} is usually unstable point.

Time τ=0 is chosen as the pump pulse delay where a induced change in Thz pulse amplitude is first observed. The THz electric field is four orders of magnitude lower than the excitation pulse electric field. Therefore, one can be sure that the THz pulse acts as a true probe pulse, not perturbing the system. One of the advantages of the THz-TDS is the distinctive detection method [27, 28]: both, the change in absorbance and the phase shift of all frequency components

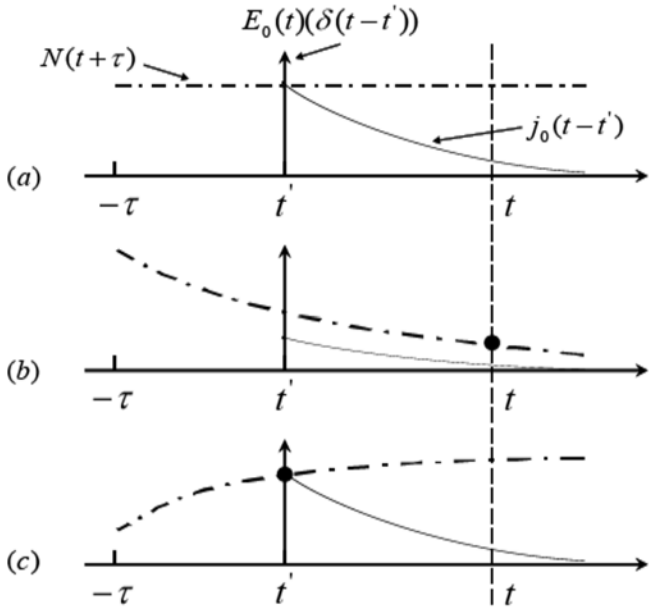

Fig. 13. Evaluation of the current (continuous light line) from the impulse by the THz field (here a delta function field $\delta(t-t')$). The current density $J(\tau,t,t')$ at a time t (vertical black, long dashed line) after excitation is separated into an amplitude function $N(t+\tau)$ (dash point line) which describes the amplitude dependence of the pump delay ($t+\tau$), and the average single particle response to the impulse field, $j_0(t-t')$. (a) When the conductivity is independent of the pump-probe delay, $N(t+\tau)$ is constant in time and the current at time t is given by $J(\tau,t,t')=Nj_0(t-t')$. (b) When the conductivity is decreasing with pump-probe delay, only the contribution of the remaining particles at time t (represented as a black dot) is to be considered and $J(\tau,t,t')= N(t+\tau)j_0(t-t')$. (c) When the conductivity is increasing with pump-probe delay, $J(\tau,t,t')$ depends on the amplitude at time t' (at the time of the impulse, again represented by the black dot), because any additional change in amplitude at later times is unaffected by the impulse field $\delta(t-t')$. Then, the current density at time t is $J(\tau,t,t')= N(t+\tau)j_0(t-t')$.

contained in the probe field are determined. This information can also be expressed in terms of complex conductivity spectrum $\sigma(\omega,\tau) = \sigma'(\omega,\tau) + i\,\sigma''(\omega,\tau)$, which is a function of the time τ after photoexcitation. The experimentally determined absorption and phase shift of the THz electric field $\Delta E(t,\tau)$ fully determine $\sigma(\omega,\tau)$ [29]. However, when $\sigma(\omega,\tau)$ changes on a time scale τ which is comparable or shorter with the THz pulse duration, the extraction of $\sigma(\omega,\tau)$ from $\Delta E(t,\tau)$ becomes more problematic, because different sample properties are probed with the beginning of the THz pulse and with his tail [20,29]. This effect must be taken into account in the data analysis.

For simplicity, it is better to consider first the case of a time-independent, constant carrier density in the sample, as depicted in Fig. 13a. In this situation, the extraction of $\sigma(\omega,\tau)$ from the experimental data is straightforward when $\sigma(\omega,\tau)$ varies slowly in time τ, during the THz probe pulse (which has a main period of about 2 ps), because this allows the definition of a quasi-steady-state conductivity $\sigma(\omega)$, [27, 30, 31]. Before taking into account the THz field used in experiments, let's first evaluate the impulse-response current $j(t)$ after an infinitely short pulsed field $E(t)=\delta(t-t')$ [32]. The impulse-response current can then be written as a product:

$$j(t) = Nj_0(t), \qquad (10)$$

where $j_0(t)$ is the single particle current-response function and N is the number of (photo-excited) charge carriers. $\sigma(\omega)$, the sample conductivity spectrum, is simply the Fourier transform of $j(t)$. When the number of photo-excited charge carriers N is not time dependent, as in this steady state approximation, $j(t)$ is proportional to $j_0(t)$, which decays in time after the impulse $\delta(t-t')$ (Fig. 13a).

The integration (Eq. 11) will then give the total current generated by an arbitrary THz pulse $E_0(t)$. $J(t)$ can also be written as a convolution between the time-independent THz field and the impulse-response current:

$$J(t) = N \int_{-\infty}^{\infty} E_0(t')\, j_0(t-t')dt', \qquad (11)$$

$$J(t) = NE_0(t) * j_0(t), \qquad (12)$$

Experimentally, the change in the transmitted THz field $\Delta E(t)$, due to photoexcitation is measured. If the sample excitation thickness is ς_{slab} and the surrounding medium has the refractive index n_{THz}, from the Maxwell equations one can derive a relation which links $\Delta E(t)$ and $J(t)$ [33]:

$$\Delta E(t) = -\frac{\varsigma_{slab}}{2\varepsilon_0 c n_{THz}} J(t), \qquad (13)$$

It should be noted that this solution is applicable only when the sample has no dispersion and the photo-induced change in the THz electric field is much smaller that this field $\Delta E(t) << E(t)$. Considering the Fourier transforms of the last two equations, the conductivity spectrum $\sigma(\omega)$ in this steady-state approximation can be obtained:

$$\sigma(\omega) = -\frac{2\varepsilon_0 c n_{THz}}{\varsigma_{slab}} \frac{\Delta E(\omega)}{E(\omega)}, \qquad (14)$$

where $E(\omega)$ and $\Delta E(\omega)$ are the Fourier transforms of the experimental data $E(t)$ and $\Delta E(t)$. The above approach is effective only when the charge carrier concentration N does not change significantly over the duration of the THz pulse (~2 ps).

Let's consider now the case of a non-steady state. The non-steady state is valid when the properties of the sample change rapidly: for example, during the excitation with the pump pulse, when the charge carriers exhibit fast trapping or recombination dynamics, or when the charges response is time dependent as a result of, for instance, carrier cooling or trapping [20, 34, 35]. In this situation one would like to extract a time-dependent conductivity $\sigma(\omega, \tau)$ [29], but the extraction of this quantity which is varying with frequency and pump-probe time in not trivial. In the simplified case of an infinitely short probe field $\delta(t-t')$, the formalism can be easily reconsidered for a density $N(t+\tau)$ decaying monotonously and simultaneously in the positive direction for both t and τ. In this case, we need to take into account the faster decay of current in the temporal region from t' to t (Fig. 13b), because changes after t' affect the experimental signal, since carriers that decay can no longer contribute to the current at time t. The contribution of $N(t+\tau)$ to the current at time t is indicated by a black dot in Fig. 13b. Expanding this

consideration for a density decaying monotonously across an arbitrary THz pulse shape, one can rewrite Eq. 12 for decreasing density:

$$J(t) = N(t,\tau)\left[E_0(t) * j_0(t)\right], \qquad (15)$$

An optical-pump THz-probe experiments allows to detect both phase and amplitude time evolution of the THz field. In this situation, as discussed in the beginning, *(t, τ)* must be measured at each pump-probe delay. Fig. 14 presents a schematic representation of the two dimensional analysis performed on data from experiments on semiconductor crystal. In the bottom part is the THz pulse before the arrival of the excitation pulse. The top plot represents the THz pulses *E(t, τ)* at different times τ after the excitation. A decrease in the amplitude of *E(t, τ)* with τ is observed, indicating a decrease in conductivity with the pump-probe delay. There is also a shift of the waveform to the left. The dashed line at a 45^0 angle represents the path of the pump pulse in the measurement: each point in a horizontal cross section *E(t)* has a different pump-probe delay. Transforming the data along this line introduces an alternative time τ' to describe the delay between the excitation pulse and all points on the probe THz pulse with the same pump delay.

To extract the time-dependent conductivity from the data, we can use a method introduced by Schmutenmaer and co-workers [20, 29]. Before Fourier transforming the time-domain data, we apply the transformation $\tau'=t+\tau$ to the last equation and obtain:

$$J_{proj}(t,\tau') = N(\tau')\left[E_0(t) * j_0(t)\right], \qquad (16)$$

The experimental data are transformed along the path of the excitation pulse (shown by dotted line in Fig. 14), all the points on a horizontal cross section of ΔE_{THz} having now the same pump-probe delay. The equivalent of Eq. 13 for the time-dependent density will then be given by:

$$\Delta E_{proj}(t,\tau') = -\frac{\varsigma_{slab}}{2\varepsilon_0 c n_{THz}} J_{proj}(t,\tau'), \qquad (17)$$

Considering the Fourier transforms of Eq. 16 and Eq. 17, the conductivity spectrum *σ(ω, τ')* can then be calculated:

$$\sigma_{proj}(\omega,\tau') = -\frac{2\varepsilon_0 c n_{THz}}{\varsigma_{slab}} \frac{\Delta E(\omega)}{E(\omega,\tau')}, \qquad (18)$$

The dependence of the pump-probe delay τ' is straightforward and represents the decay of the charge-carrier population. The frequency-dependent part corresponds to the response of an infinitely long-lived charge carrier. However, Eq. 14 to Eq. 18 do not take into account the new charge carriers which might be created during or after the THz pulse. This situation is most easily depicted again for a delta function probe field *δ(t−t')* (Fig. 13c). When the density is increasing between t_0 and t, the additional charges are not probed by the field at time *t'* and hence do not contribute to any current at time *t*. The relevant density for calculating the current will then be *N(t'+τ)* instead of *N(t+τ)*. However, the introduction of *t'* dependence in *N* means that the equivalent form of Eq. 13 for increasing density is not a simple convolution and interpretation of the extracted conductivity spectrum is not straightforward. In other words the transformation

one apply to the data does give complex results when the pump and THz pulse overlap and need to be address as special case of 2D-Raman process.

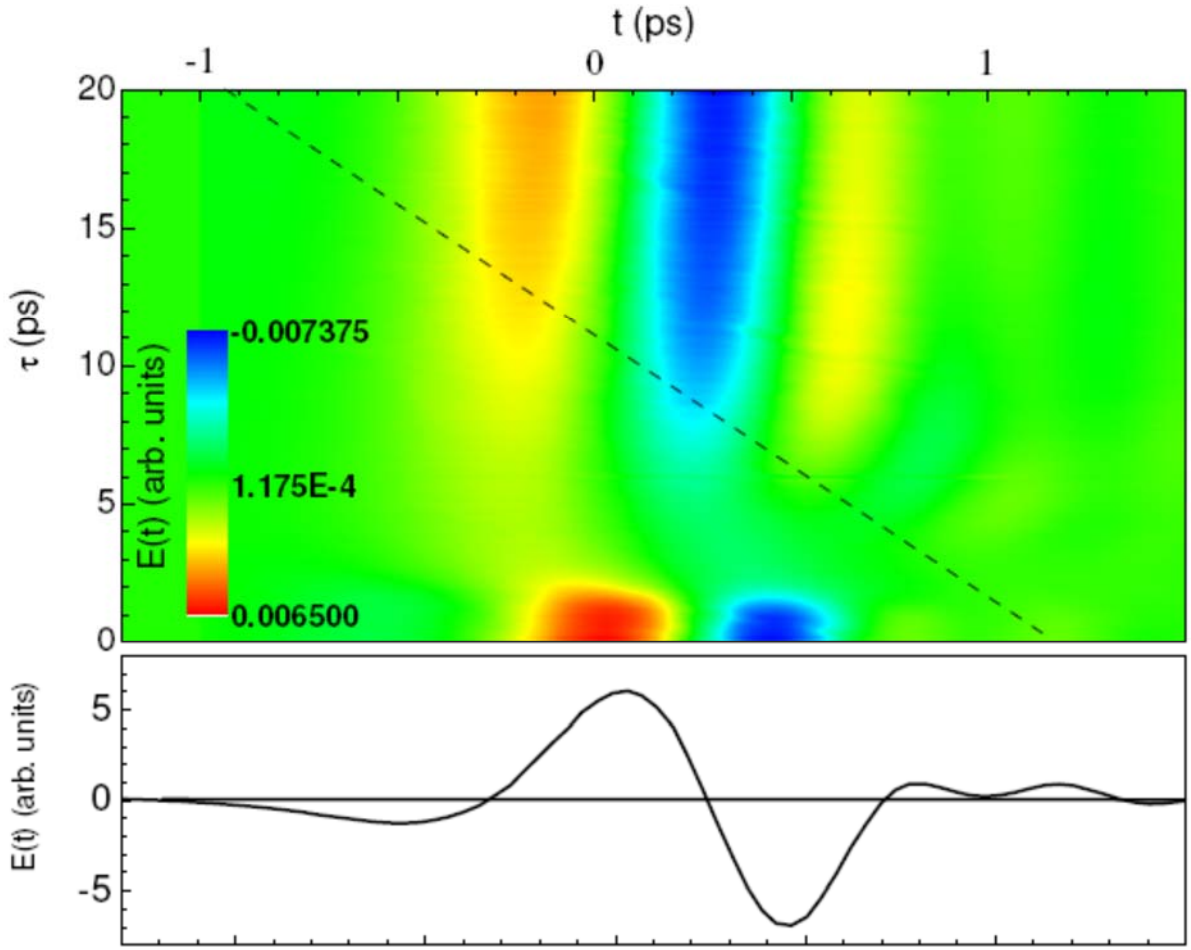

Fig. 14. A measurement taken on a copper oxide sample. In the bottom part is the THz pulse before the arrival of the excitation pulse. The top plot represents the the THz pulses E(t,t) at different times τ after the excitation. A decrease in the amplitude of E(t, τ) with τ is observed, indicating a decrease in conductivity with the pump-probe delay. There is also a shift of the waveform to the left. The dashed line at a 45^0 angle represents the path of the pump pulse in the measurement: each point in a horizontal cross section E(t) has a different pump-probe delay. Transforming the data along this line introduces an alternative time τ' to describe the delay between the excitation pulse and all points on the probe THz pulse with the same pump delay.

1. N. Nagai, R. Shimano, and M.K. Gonokami, Physical Review Letters, 86, 5795 (2001)
2. J.T. Kindt and C.A. Schmuttenmaer, J. Phys. Chem., 100, 10373 (1996)
3. C. Ludwig and J. Kuhl, Appl. Phys. Lett., 69, 1194 (1996)
4. P.R. Smith, D.H. Auston, and M.C. Nuss, IEEE J. QUantum Electron., 24, 255 (1988)
5. X.C. Zhang, B.B. Hu, J.T. Darrow, and D.H. Auston, Appl. Phys. Lett., 56, 1011 (1990)
6. D.J. Cook and R.M. Hochstrasser, Opt. Lett., 25, 1210 (2000)
7. H. Hamster, A. Sullivan, S. Gordon, W. White, and R.W. Falcone, Physical Review Letters, 71, 2725 (1993)
8. Q. Chen, Z.P. Jiang, M. Tani, and X.C. Zhang, Electron. Lett., 36, 1298 (2000)
9. P.Y. Han, M. Tani, F. Pan, and X.C. Zhang, Opt. Lett., 25, 675 (2000)
10. J.J. Carey, R.T. Bailey, D. Pugh, J.N. Sherwood, F.R. Cruickshank, and K. Wynne, Appl. Phys. Lett., 81, 4335 (2002)
11. C. Kubler, R. Huber, S. Tubel., and A. Leitenstorfer, Appl. Phys. Lett., 85, 3360 (2004)
12. K. Reinmann, R.P. Smith, A.M. Weiner, T. Elsasser, and M. Woerner, Opt. Lett., 28, 471 (2003)
13. P.Y. Han, G.C. Cho, and X.C. Zhang, J. Nonlinear Opt. Phys. Mater., 8, 89 (1999)
14. P. Jepsen, J. Shan, A.S. Weling, E. Knoesel, L. Bartels, M. Bonn, A. Nahata, G.A. reider, and T.F. Heinz, Opt. Lett., 25, 426 (2000)
15. Z.P. Jiang and X.C. Zhang, Opt. Lett., 23, 1114 (1998)
16. P. Jepsen, Z.P. Jiang, and X.C. Zhang, Appl. Phys. Lett., 72, 1945 (1998)
17. P. Jepsen, F.G. Sun, Z.P. Jiang, and X.C. Zhang, Appl. Phys. Lett., 73, 2233 (1998)
18. P. Jepsen, A. Nahata, and T.F. Heinz, Opt. Lett., 23, 67 (1998)
19. Q. Chen and X.C. Zhang, Appl. Phys. Lett., 68, 1604 (1996)
20. M.C. Beard, G.M. Turner, and C.A. Schmuttenmaer, Phys. Rev. B, 62, 15764 (2000)
21. Q. Wu, M. Litz, and X.C. Zhang, Appl. Phys. Lett., 68, 2924 (1996)
22. A. Nahata, D.H. Auston, and T.F. Heinz, Appl. Phys. Lett., 68, 150 (1996)
23. A. Nahata, A.S. Weling, and T.F. Heinz, Appl. Phys. Lett., 69, 2321 (1996)
24. K.H. Yang, P.L. Richards, and Y.R. Shen, Appl. Phys. Lett., 19, 285 (1971)
25. P. Jepsen, C. Winnewisser, M. Schall, V. Schyja, S.R. Keyding, and H. Helm, Phys. Rev. E, 53, 3052 (1996)
26. P. Jepsen and B.M. Fischer, Opt. Lett., 30, 29 (1993)
27. M.C. Beard, G.M. Turner, and C.A. Schmuttenmaer, J. Phys. Chem., 106, 7146 (2002)
28. G. Gallot and D. Gischkowsky, J. Opt. Soc. America B, 16, 1204 (1999)
29. J.T. Kindt and C.A. Schmuttenmaer, J. Chem. Phys., 110, 8589 (1999)
30. E. Knoesel, M. Bonn, J. Shan, F. Wang, and T.F. Heinz, J. Chem. Phys., 121, 394 (2004)
31. J. Shan, F. Wang, E. Knoesel, and T.F. Heinz, Phys. Rev. Lett., 90, 247401 (2003)
32. N.V. Smith, Phys. Rev. B, 64, 155106 (2001)
33. H.K. Nienhuys and V. Sundstrom, Phys. Rev. B, 71, 235110 (2005)
34. E. Hendry, J.M. Schins, L.P. Candeias, L.D.A. Siebbeles, and M. Bonn, Phys. Rev. Lett., 92, 196691 (2004)
35. M.C. Beard and C.A. Schmuttenmaer, J. Chem. Phys., 114, 2903 (2001)